Vibrational properties of nanometric AB_2 ionic clusters

B Montanari[1,4]**, P Ballone**[2]**, T Mazza**[3] **and P Milani**[3]

[1] CCLRC Rutherford Appleton Laboratory, Chilton Didcot, Oxfordshire OX11 0QX, UK
[2] Dipartimento di Fisica, Università di Messina, Contrada Papardo, I-98166 Messina, Italy
[3] CIMAINA and INFM—Dipartimento di Fisica, Università di Milano, via Celoria 16, I-20133 Milano, Italy

E-mail: B.Montanari@rl.ac.uk

Abstract
A broad survey of harmonic dynamics in AB_2 clusters with up to $N = 3000$ atoms is performed using a simple rigid ion model, with ionic radii selected to give rutile as the ground state structure for the corresponding extended crystal. The vibrational density of states is already close to its bulk counterpart for $N \sim 500$, with characteristic differences due to surfaces, edges and vertices. Two methods are proposed and tested to map the cluster vibrational states onto the rutile crystal phonons. The net distinction between infrared (IR) active and Raman active modes that exists for bulk rutile becomes more and more blurred as the cluster size is reduced. It is found that, in general, the higher the IR activity of the mode, the more this is affected by the system size. IR active modes are found to spread over a wide frequency range for the finite clusters. Simple models based on either a crude confinement constraint or surface pressure arguments fail to reproduce the results of the calculations. The effects of the stoichiometry and dielectric properties of the surrounding medium on the vibrational properties of the clusters are also investigated.

(Some figures in this article are in colour only in the electronic version)

1. Introduction

The recent, fast growth in the field of nanostructured and cluster-assembled materials has boosted the interest in the investigation of ionic clusters by experimental and theoretical methods, which can now both benefit from the advancements in the techniques for their synthesis and characterization.

[4] Author to whom any correspondence should be addressed.

Ionic crystals are among the best understood condensed matter systems, since their interatomic forces are fairly well known, and several of their structural and dynamical properties have been clarified long ago [1]. The properties of ionic clusters, however, have been investigated to a much lesser extent. Early theoretical studies of their morphological and dynamical properties focused mainly on the micrometre size scale, and are relevant for all sizes for which an elastic continuum model is justified [2–5]. Since the early days of computer simulation, atomistic models based on Born–Mayer potentials have been used to investigate sub-nanometric ionic clusters [6]. The recent, fast progress in first principles computations has spurred several investigations, based on density functional theory (DFT), of very small ionic clusters (up to a few tens of atoms) [7]. Reaching the mesoscopic range that is relevant in most materials science applications purely with first principles methods remains challenging. The present work, which discusses the dynamical properties of ionic clusters of low-nanometric sizes (from 480 up to 3000 atoms), narrows the gap between the elastic continuum models of early studies and the atomistic view increasingly required to describe systems whose size is progressively reduced.

The primary aim of this study is to provide a preliminary but broad survey of dynamical properties of AB_2 ionic clusters, which recently enjoyed a renewed experimental interest. Our computations, in particular, were stimulated by the structural and vibrational characterization of cluster-assembled rutile TiO_2 films [8, 9], which motivates the emphasis on the rutile phase given in the present study, even though ionic AB_2 materials (and clusters [10][5]) are known to adopt a wide variety of different structures. Based on the computations, the validity of simple confinement models used to relate clusters and bulk vibrational frequencies is tested. In addition, this study also investigates the dielectric properties of the clusters, and the influence of the stoichiometry and of the medium in which the clusters are embedded.

No real system is purely ionic, and AB_2 systems are far from the simplicity of alkali halides. The quantitative description of systems such as TiO_2, in particular, cannot neglect the electronic polarizability and the residual covalent character of its interatomic interactions. First principles DFT simulations for systems of thousands of atoms and electrons are already possible although still severely limited in scope. In the meantime, a large number of empirical potential models have been developed for AB_2 systems (including TiO_2 [11]), and applied to the investigation of structural and dynamical properties in a variety of different conditions, including clusters [12]. Bulatov *et al*, for instance, computed low-frequency oscillations in nanoclusters of lanthanum trifluoride [13] and found that quite small clusters (up to 3120 atoms) already show features described by models that treat the cluster as a continuum. Vyas *et al* [14] compared the surface structures obtained from molecular dynamics (MD) simulations of equally small clusters of CaF_2 to those obtained with static 2D energy minimizations and found little difference. Despite the rapid improvement of these competing and arguably more sophisticated methods, a broad survey of dynamical properties by a general model that uses the bare minimum of parameters still provides important clues to understanding the major features and trends observed in experimental results. For this reason, a simple rigid ionic model is employed here.

This paper is organized in the following way. The next section describes the model potential chosen for the calculations, the techniques used for the geometry optimization, and the method for computing the vibrational properties. Section 3 describes the equilibrium geometries of the clusters. Section 4.1 presents the dynamical properties of the clusters obtained from the calculations and compares them with those given by simple confinement

---

[5] Titania (TiO_2) nanocrystals produced by popular industrial processes (sol–gel and aerosol) are found in the anatase structure, transforming to rutile upon annealing at $T \sim 1000$ K; see [10]. Titania clusters can be produced directly in the rutile phase by the method described in [8].

models. The dielectric properties of the clusters are described in section 4.2. Sections 4.3 and 4.4 describe the effects of stoichiometry and of the environment on the vibrational spectra of the clusters. The main conclusions of this work are summarized in section 5.

2. Computational details

Systems made by two ionic species (A and B) of charge $Z_A = 2$ and $Z_B = -1$ are considered here, whose ions interact via the potential energy:

$$U(R) = \frac{1}{2} \sum_{i \neq j=1}^{N_A+N_B} \frac{Z_i Z_j}{|\mathbf{R}_i - \mathbf{R}_j|} + \sum_{i=1}^{N_A} \sum_{j=N_A+1}^{N_A+N_B} \left(\frac{\sigma_{AB}}{|\mathbf{R}_i - \mathbf{R}_j|} \right)^{12} + \frac{1}{2} \sum_{i \neq j=N_A+1}^{N_A+N_B} \left(\frac{\sigma_{BB}}{|\mathbf{R}_i - \mathbf{R}_j|} \right)^{12}, \quad (1)$$

where it has been assumed that positive ions are numbered from 1 to N_A, and negative ions from $N_A + 1$ to $N_A + N_B$. All quantities are expressed in terms of unspecified charge, length and mass units (defining the time and energy units), which can be selected in order to approach any specific AB$_2$ system. Numerical results, therefore, represent relative quantities, and, as such, they will be treated as dimensionless. The short-range repulsion for A–A pairs is neglected since the strong Coulomb repulsion already prevents close encounters for the ions of highest charge. For the sake of simplicity, both species are assumed to have the same mass $M = 1$. By identifying the σ_{AB} parameter with the nearest-neighbour distance of real AB$_2$ systems, it turns out that the nanometric range for clusters starts at about one hundred atoms, extending up to a few million. The largest cluster investigated here ($N = 3000$), in particular, has a diameter $D = 8$ nm if σ_{AB} is set to 1.96 Å, corresponding to the average equilibrium Ti–O nearest-neighbour separation in bulk TiO$_2$ rutile.

The large disparity between D and the wavelength of light $\lambda (D \ll \lambda)$ implies that retardation effects can be neglected, and the cluster interaction with electromagnetic waves can be discussed in terms of the harmonic dynamics of the cluster ions [2]. Only for much larger samples ($D \geqslant \lambda$) do retardation effects become important, and polaritons (normal modes having a photon as well as a phonon component) take over as the relevant elementary excitation [15].

Even with the drastic restriction of the analytic form for the potential energy given by equation (1), the T, $P = 0$ phase diagram of the model as a function of σ_{AB} and σ_{BB} is remarkably complex, as it displays a large number of different crystal structures. For the current study the ionic radii are chosen to be $\sigma_{AB} = 1.4$ and $\sigma_{BB} = 1.8$, which lead to a model with rutile as the bulk equilibrium structure and with several other low energy structures known to occur for TiO$_2$.

The determination of the equilibrium configuration of a many-atom system is known to be a challenging problem in all but the simplest cases. In the case of clusters, the space filling constraint that restricts the symmetries of crystals is removed, and a very wide variety of structures can occur, leading to an NP-complete combinatorial problem (see [16]). In the nanometric range, however, the local arrangement of atoms is already expected to reflect that of the corresponding extended crystal at least in the core region. In the micrometre range the shape of crystallized samples can be predicted by the Wulff construction [17]. The relevance of this macroscopic recipe in the nanoscale range is, however, far less established.

The structural optimization is addressed here with three different methods, all based on simulated annealing (SA) coupled with: (1) molecular dynamics on the continuum (MD-SA), (2) Monte Carlo on a discrete lattice model (MC-SA), and (3) a genetic algorithm (GA-SA), using quenched MD to locate local energy minima.

The geometries resulting from the longest MD-SA performed[6] ($\sim 60 \times 10^6$ time steps) are clearly amorphous, with an energy per AB_2 molecule much higher than that of the rutile crystal (even when an estimated surface contribution is added), and with a local atomic coordination that qualitatively differs from that of rutile.

The MC-SA method on a discrete lattice model is used to force crystallization. In this method, the ions move only on the sites of a finite rutile lattice, whose size is about eight times larger than that of the actual cluster, and whose lattice constant is kept at the bulk equilibrium value. Positive (A) and negative (B) ions move only on their (A or B) respective sublattices. At each temperature, the system is equilibrated by a Monte Carlo procedure that includes single ion moves, whole AB_2 molecule displacements, AB_2 rotations and bending variations[7]. The simulations start at a temperature such that the ions are spread over the whole rutile lattice available, and then the temperature is slowly reduced down to $T = 0$. This stage of the optimization takes about 2×10^5 attempted MC moves per ion. The structures obtained by MC-SA are then relaxed by using MD on the continuum, and further optimized via a low temperature SA (with T up to 0.005), in order to activate possible surface reconstructions. The final structures are clearly recognizable as (defective) rutile nanograins, and their potential energy is significantly lower than that of the clusters optimized by MD-SA.

The third optimization method tried here is GA-SA [18], whose performance is explored for a cluster containing 1056 ions. Twenty five initial (amorphous) geometries are selected at random from a low temperature MD trajectory. Successive generations are produced by the following steps.

(a) A unit vector **n** is selected with random orientation.

(b) The cluster is cut into two parts by a plane perpendicular to **n** and going through the cluster centre of mass.

(c) The two cluster halves are rotated by a random angle $\phi \in [0; 2\pi]$.

(d) The rotated structures are locally optimized by quenched MD[8].

(e) Each of the resulting clusters is propagated to the following generation with probability proportional to $\exp[-E/T]$, where E is the cluster energy, and T is a reference temperature that is progressively reduced. The total population is kept fixed at 25 clusters.

This procedure was not able to produce clusters with an energy competitive with the lowest energy given by the MC-SA strategy.

The results confirm that the geometry optimization of clusters made of a few hundred atoms is an exceedingly difficult problem, with no clear and general strategy able to provide a reliable solution over a wide variety of model parameters.

Starting from the geometry-optimized rutile clusters, the dynamical matrix elements are computed by finite difference differentiation of the potential energy with respect to the ionic positions. Finally, the harmonic vibrational frequencies and eigenvectors are determined by diagonalizing the dynamical matrix.

---

[6] Molecular dynamics simulations are performed with a time step $\delta t = 0.01$.

[7] AB_2 molecules are identified simply by pointing at a positive ion, and verifying whether this is at least two-fold coordinated. In the case of a positive answer, two negative nearest neighbours are selected at random to complete the neutral AB_2 molecule. Rotations and bending variations are limited to the discrete choices imposed by the rutile lattice.

[8] Quenched molecular dynamics is performed by moving ions according to standard constant energy MD. Velocities are set to zero whenever the scalar product of velocities and forces becomes negative. It is easy to verify that this procedure gives a monotonically decreasing potential energy.
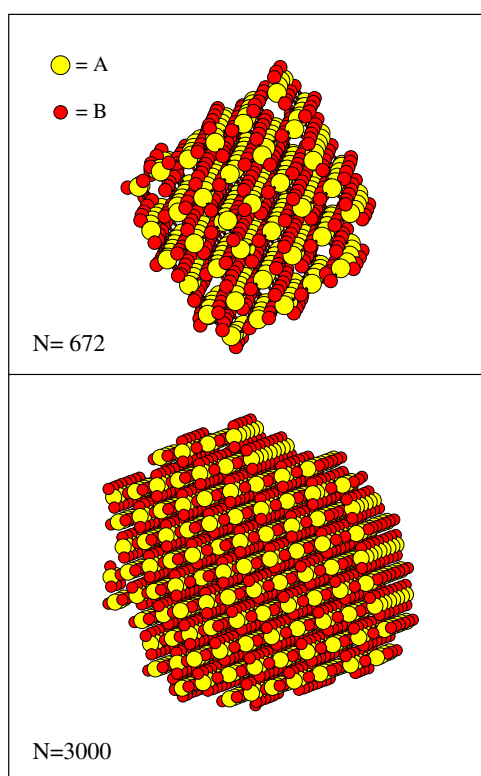
Figure 1. Lowest energy structures found by the MC-SA method for $N = 672$ and 3000.

3. Equilibrium structures

The model described in the previous section has rutile as its lowest energy crystal form at $P = 0$, with a cohesive energy $E_c^{\text{bulk}} = 0.4153$ per molecule with respect to the constituent AB$_2$ molecules. In qualitative agreement with the TiO$_2$ phase diagram, the anatase structure is slightly less stable ($E_c^{\text{bulk}} = 0.4011$), followed by brookite ($E_c^{\text{bulk}} = 0.3963$).

Structural optimizations with the method described in section 2 are carried out for nine cluster sizes, i.e., $N = N_A + N_B = 480, 672, 1056, 1080, 1650, 1980, 2376, 2808$, and 3000.

The resulting structures are illustrated in figure 1 for $N = 672$ and 3000. As expected, the clusters' shapes only partially reflect the predictions of the Wulff construction (see [19]). On the one hand, the low energy (110) surface is indeed and by far the most represented surface for all cluster sizes. On the other hand, the contribution of other crystallographic surfaces is difficult to assess and quantify, because their limited extension and evident distortions make their identification rather ambiguous. Moreover, while the core region of each cluster is well ordered (clusters are stoichiometric by construction), defects are present at the surface, especially at edges and vertices. The observed surface disorder could be due to the practical limitations of the optimization strategy, but it might also reflect in a realistic way entropy effects relevant at the temperatures at which clusters condense and crystallize.

In analogy with the case of the homogeneous crystal, the cohesive energy E_c of each cluster is computed with respect to the total energy of $(N_A + N_B)/3$ isolated AB$_2$ molecules.
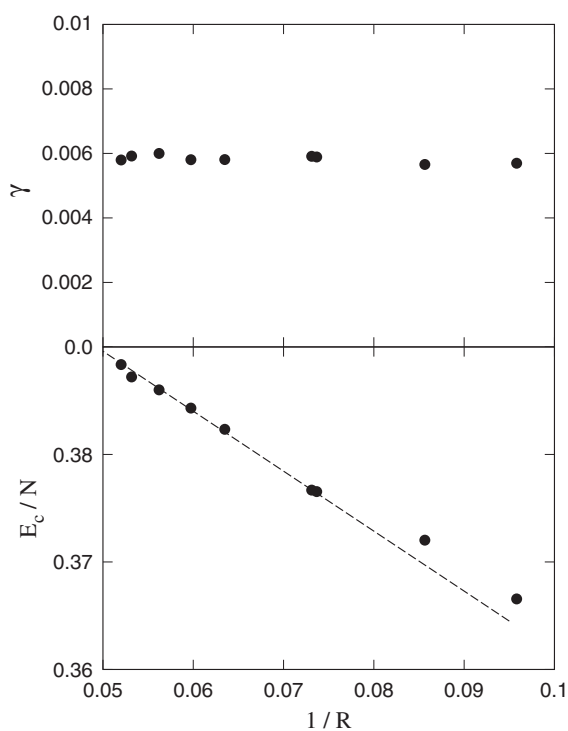
Figure 2. Lower panel: cohesive energy E_c per molecule for the optimized clusters as a function of the inverse radius $1/R$. The cohesive energy is computed with respect to the total energy of an isolated AB_2 molecule. Upper panel: surface energy γ of rutile clusters as a function of the inverse cluster radius $1/R$. The ground state energy and volume of an homogeneous rutile crystal have been used to define the cluster radius (R) and surface energy (see text).

In addition, the surface energy γ is determined by equating $4\pi R^2 \gamma$ with the cohesive energy difference between the cluster and an equal number of molecules in the rutile bulk. The cluster radius R is defined by the relation

$$\frac{(N_A + N_B)}{3} V(AB_2) = \frac{4\pi}{3} R^3, \tag{2}$$

where $V(AB_2) = 2.281$ is the equilibrium volume per molecule of bulk rutile. Cohesive (E_c) and surface (γ) energies as a function of $1/R$ are shown in figure 2. It is evident that already in this size range the dependence of both quantities on size closely follows the predictions of macroscopic surface thermodynamics [17].

The electrostatic dipole moment of the optimized clusters is small but not completely negligible. The modulus of the total moment is nearly independent of size, resulting in a dipole *per* AB_2 *molecule* that decreases as $\sim 1/R^3$ (from $|d| = 0.02$ per molecule for $N = 480$ to $|d| = 0.0042$ per molecule in the case $N = 3000$) with increasing cluster size.

The convergence of the cluster properties to their correct bulk limit confirms that the set of optimized structures determined in the present study is indeed representative of the growth sequence for this model system.
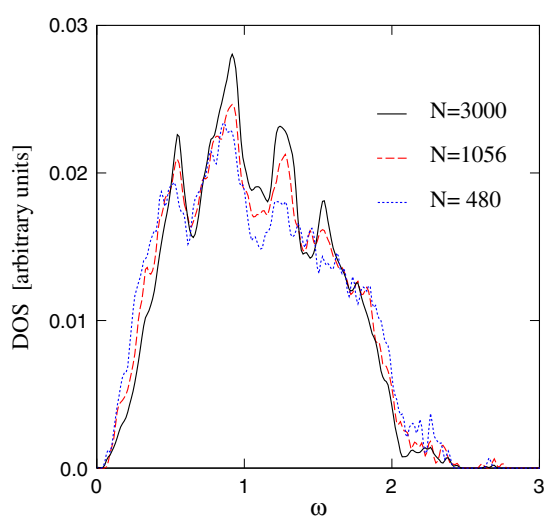
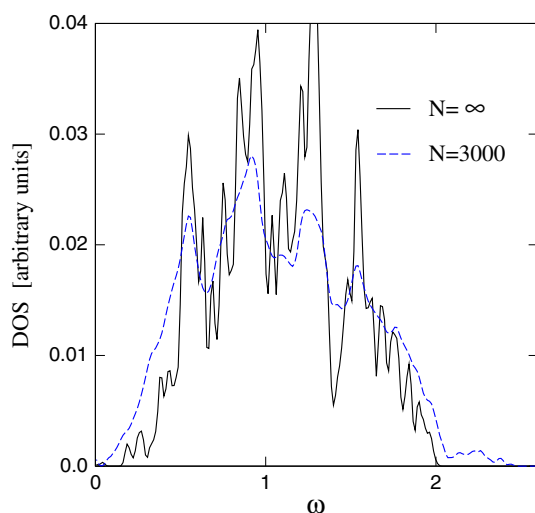**Figure 3.** Size dependence of the vibrational density of states.

Figure 4. Comparison of the vibrational DOS for the optimized $N = 3000$ cluster (dashed line) and for bulk rutile (full line).

4. Harmonic dynamics

4.1. Stoichiometric rutile clusters

The size dependence of the density of states (DOS), $D(\omega)$, is illustrated in figure 3, and the DOS for the $N = 3000$ cluster is compared to the result for bulk rutile in figure 4. Based on computational considerations, one would calculate the bulk density of states by using the primitive unit cell and sampling the system's first Brillouin zone. Here a different approach is used, whereby an approximate DOS is computed by using the Γ-point vibrational modes of a large supercell (1944 atoms) in order to approach the geometrical discretization found

in clusters, thus highlighting the role of structural and force constants changes in going from the bulk to nanoclusters. This large supercell is periodically repeated in space, and the Ewald technique is used to account for long-range Coulomb interactions. The data are normalized in such a way that for all sizes $\int_0^\infty D(\omega)\,d\omega = 1$. It is clear that the main qualitative features characterizing the rutile crystal DOS are already present in the $D(\omega)$ for the $N = 480$ sample. Systematic changes occur as the cluster size increases, leading to a better definition of peaks and valleys in $D(\omega)$. Quantitative differences, however, are small over the $N = 480$–3000 size range, while the DOS for the largest cluster ($N = 3000$) is still markedly distinct from that of bulk rutile.

These observations suggest that basic vibrational properties arise very early along the clusters' growth sequence, reflecting the dominant role of geometrical packing and long-range Coulomb forces. The final convergence of dynamical properties to their bulk limit, however, is slow, taking place over a size range extending much beyond the limited domain accessible to simulation. A better understanding of vibrational properties of clusters can be obtained by identifying features that are directly connected to bulk phonons, and features that are instead related to surfaces and surface defects.

We first analyse the vibrational modes that have a clear bulk counterpart. Their evolution along the clusters sequence can be seen as an essential size dependence, related to phonon confinement. The comparison between cluster and bulk vibrational modes is made possible by the remarkable degree of crystal-like order observed in the local atomic arrangement of clusters, significantly perturbed only at edges and vertices. Because of this ordering (perhaps slightly enhanced by our optimization strategy) it is possible to assign almost every atom in each cluster to one of the six atoms in the unit cell of bulk rutile. It is therefore possible to compare displacement patterns for the bulk and for the clusters. In the case of Γ-point phonons, for instance, two recipes were explored for comparing cluster and bulk vibrations, both giving qualitatively similar results.

The first recipe consists in projecting the cluster vibrational eigenvectors $\{\mathbf{v}^\alpha, \alpha = 1, \ldots, 3N\}$ on each of the 18 Γ-point phonons $\{\mathbf{u}_\Gamma^\beta, \beta = 1, \ldots, 18\}$ of rutile. This is made possible by the identification of each ion in the cluster with one of the six ions in the rutile unit cell. Then, a plot of $|\langle \mathbf{v}^\alpha | \mathbf{u}_\Gamma^\beta \rangle|^2$ as a function of ω_α provides a measure of the energy spread due to confinement for the Γ-point phonon β. In this plot it is also possible to associate an approximate IR, Raman or silent character to the different peaks in the cluster DOS. It should be noted that the strict separation of IR active and Raman active modes that is imposed by the symmetry in bulk rutile becomes blurred for the clusters as a consequence of symmetry loss. Two major cases are observed. In the case of IR active modes, the fragmentation of the original Γ-point phonon is a major effect (see figure 5(a)), as one would expect for modes driven by long-range Coulomb forces. All these modes spread over the same energy interval ($1 \leqslant \omega \leqslant 1.5$), and are significantly hybridized. The size dependence of $|\langle \mathbf{v}^\alpha | \mathbf{u}_\Gamma^\beta \rangle|^2 (\omega_\alpha)$ is mild over the $N = 672$–3000 size range, suggesting that convergence to the macroscopic limit is particularly slow for the IR active component of the spectrum.

At variance with the IR active modes, Raman active and silent modes conserve their identity in going from the bulk down to the lowest sizes considered in the present study. These Γ-point bulk phonons in the clusters transform into fairly narrow lines, superimposed to a broad but quantitatively unimportant background. The half-width at half-maximum reaches 0.075 (energy units) at the lowest sizes, and decreases slowly but regularly with increasing N. In a few cases, an intermediate pattern is observed, where a Raman active or silent Γ-point phonon is fragmented into two or more peaks, usually of unequal width and height (see figure 5(c)). In both the (a) and (c) cases, attempts to define a size-dependent frequency for each of the Γ-point phonons were unsuccessful.
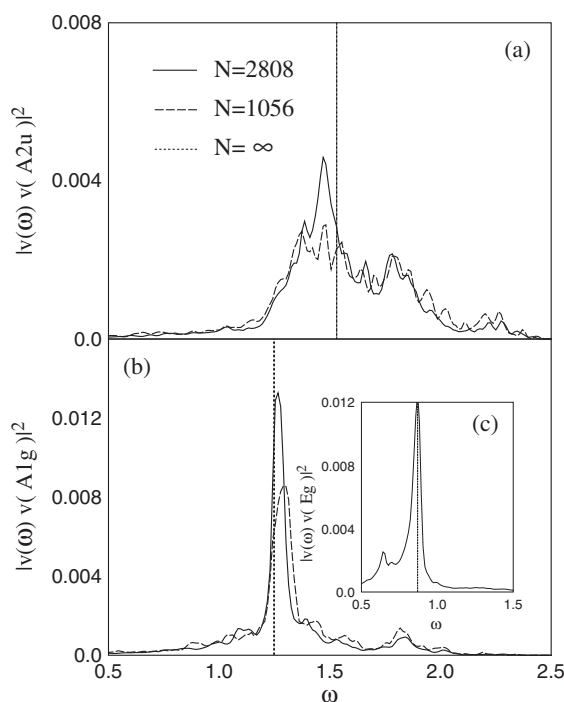
Figure 5. Square modulus of the projection of cluster vibrational modes on Γ-point bulk rutile phonons (see text). Full line: $N = 3000$. Dashed line: $N = 1056$. Vertical line: bulk rutile.

A more systematic and quantitative picture is provided by the second recipe, which consists in defining a reduced 18×18 dynamical matrix ($Q_{\alpha\beta}$; $\alpha, \beta = 1, \ldots, 18$) for clusters, converging to the Γ-point dynamical matrix of rutile in the bulk limit. Each of its 18 dimensions corresponds to the simultaneous displacement of all cluster ions belonging to the same rutile ion type along one Cartesian coordinate. Also, in this case, the crucial step is the unambiguous identification of each ion in the cluster with one of the six ions in the rutile unit cell. A quantitative analysis of the relation between bulk Γ-point phonons and the eigenvalues and eigenvectors of $Q_{\alpha\beta}$ is reported in the appendix.

The computed frequencies of $Q_{\alpha\beta}$ depend linearly on the inverse cluster radius $1/R$, as shown in figure 6. The coefficients $\omega(\infty)$ and a of a linear fit ($\omega(R) = \omega(\infty) + a/R$) to the computational results are shown in table 1. In all cases, the $1/R \longrightarrow 0$ limit $\omega(\infty)$ is very close to the bulk phonon frequency computed using a crystal unit cell and periodic boundary conditions. The coefficient a, which measures the size dependence of each frequency, displays large differences (up to more than one order of magnitude) among different modes. Moreover, contrary to the intuitive idea that confinement always raises frequencies because of its effect on the kinetic energy contribution, the sign of a is negative for some modes. The average $|a|$ is twice as large for IR active than for Raman active modes. However, the largest shifts due to confinement (~10% of the bulk value in the $N = 672$–3000 size range) seem to be nearly equally distributed among infrared, Raman and silent modes. The shifts computed by this method agree at least qualitatively with those provided by the first method for Raman active and silent modes, which give rise to sharp lines in the projection recipe discussed above.
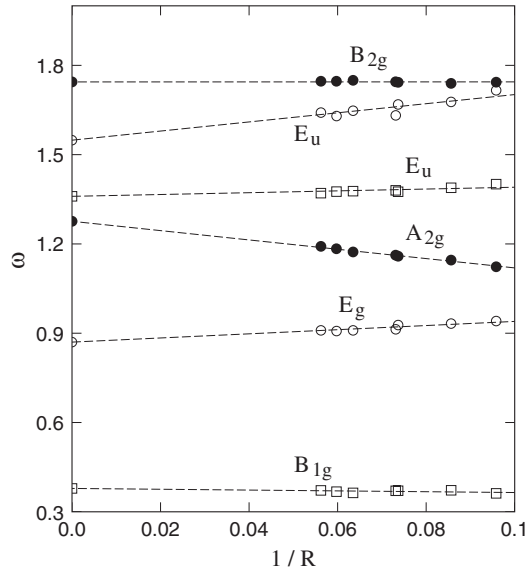
Figure 6. Square root of the eigenvalues of the 18×18 reduced matrix $Q_{\alpha\beta}$, converging to the Γ-point dynamical matrix in the $1/R \longrightarrow 0$ limit (see text). The dashed lines are a linear interpolation to the computational data. Their linear coefficient is reported in table 1.

Table 1. Size dependence of the frequency, ω, of cluster modes adiabatically connected to rutile Γ-point phonons. $\omega(\infty)$ and a are the coefficients of a linear fit ($\omega(R) = \omega(\infty) + a/R$) to the computational data. R is the cluster size defined by equation (2). The IR, R and S labels refer to the infrared, Raman or silent character of each bulk mode, respectively.

Mode	B_{1g}(R)	B_{1u}(S)	E_g(R)	E_g(R)	E_u(IR)	E_u(IR)	A_{1g}(R)	A_{2g}(S)
$\omega(\infty)$	0.378	0.789	0.870	0.870	1.092	1.092	1.248	1.276
a	-0.137	-0.420	0.591	0.696	-0.668	-0.663	1.310	-1.566

Mode	B_{1u}(S)	E_u(IR)	E_u(IR)	A_{2u}(IR)	E_u(IR)	E_u(IR)	B_{2g}(R)
$\omega(\infty)$	1.300	1.360	1.360	1.531	1.549	1.549	1.744
a	1.608	0.190	0.306	0.911	1.323	1.533	0.002

Two simple models are applied here that predict the evolution of the vibrational properties as a function of the clusters' size based on the knowledge of the bulk vibrational modes. The first model is a very simple confinement model which assumes that the (real space) wavefunction of the cluster vibrational modes is given by plane waves modulated by a size-dependent confinement function [20–24]. In the case of a Γ-point phonon, for instance, this gives

$$\Phi(\mathbf{r}) = f(\mathbf{r}, N)u(\mathbf{r}), \tag{3}$$

where f is roughly one within the cluster volume, and zero outside; u is a function with the rutile lattice periodicity. Analytic results for the frequency shift and the broadening of each Γ-point phonon can be obtained by further assuming that

$$f(\mathbf{r}, N) \sim \exp[-8\pi^2 r^2/R^2], \tag{4}$$

where R is the cluster radius defined in equation (2). Then, the original bulk rutile phonon

gives rise to a broadened line whose frequency dependence is

$$I(\omega) = \int_{BZ} \frac{\exp[-q^2 R^2/16\pi^2]\, d\mathbf{q}}{[\omega - \omega(\mathbf{q})]^2 + (\delta/2)^2}, \tag{5}$$

where the integral extends over the Brillouin zone (BZ), $\omega(\mathbf{q})$ is the bulk phonon dispersion relation, and δ is a suitable (small) bulk line width ($\delta = 0.001$). In other words, the cluster confinement mixes phonons whose $\mathbf{q}$ vector is not exactly zero, although their weight in the cluster eigenstate decreases rapidly with increasing q^2. Then, the frequency shift and the broadening implicit in equation (5) can be computed by replacing the full phonon dispersion relation by a Taylor expansion around Γ up to quadratic terms. An explicit computation based on numerical data for the phonon dispersion relations provides results that are quantitatively and often qualitatively different from those given by the computational recipes discussed above. The failure of the simple confinement model is probably due to the fact that it neglects the mixing of different Γ-point modes of appropriate symmetry, which is made possible by the finite size of the clusters. Moreover, this model does not include the change of force constants in going from the bulk to the cluster, which, although limited to the surface layers, is an all-important feature in nanometric systems.

The second simple scheme assumes that the peaks in the vibrational DOS of the clusters are those of the bulk modified by the effect of the surface pressure. This model is based on the well known Laplace equation, i.e., $\Delta P = 2\Psi/R$, which states the equivalence of the surface tension, Ψ, with an external pressure acting on a finite sample of radius R (see [17]). Then, the size dependence of the vibrational frequencies is attributed to their pressure dependence. This model has the advantage of predicting in a transparent way the $1/R$ linear dependence of frequency on size. To test this model, the pressure derivative of the Γ-point phonons of rutile has been computed by numerical differentiation. These data, together with the surface energy γ shown in figure 2[9], are used to predict the linear coefficient $d\omega/d(1/R)$. Once again, the results disagree quantitatively and sometimes qualitatively with the data provided by our computational investigation. Obviously, the pressure effect due to the surface tension is one of the factors influencing vibrational frequencies, but clearly this is not the major player. Moreover, the anisotropy of the rutile lattice might require a complex extension of the model that has not been attempted here, and that would be of limited interest for applications.

In addition to modes adiabatically connected to rutile bulk phonons, the vibrational spectrum of clusters includes modes whose existence strictly depends on the finite size of the system. The comparison of the cluster and bulk DOS (see figure 4) shows where these states are to be found. The clusters display a clear DOS excess at very low ($\omega \leqslant 0.5$) and very high ($\omega \geqslant 1.8$) frequency. Moreover, the cluster DOS shows an accumulation of surface localized states in the dips of the rutile crystal DOS. These qualitative considerations are quantified by the following procedure. First, all atoms whose first coordination shell is incomplete (AB pairs only are considered) are classified as *surface* atoms. Strictly speaking this definition is too simplistic, but the major exceptions to this rule are due to vacancies within the cluster, whose concentration is negligible. Second, the surface localization of each mode α is measured by the function $P_{\text{surf}}(\alpha)$, defined as the square modulus of the displacement vector for the surface atoms. By construction $0 \leqslant P_{\text{surf}}(\alpha) \leqslant 1$, the values of $P_{\text{surf}}(\alpha)$ close to one correspond to surface localized modes, while $P_{\text{surf}}(\alpha) \sim 0$ identifies modes spread over the entire cluster. The results for $N = 3000$ are shown in figure 7, and they confirm that both the highest and lowest frequency modes are surface localized. Moreover, a peak

---

[9] At $T = 0$ surface energy and surface tension are numerically equal for isotropic materials. Their relation, however, is more involved for anisotropic solids.
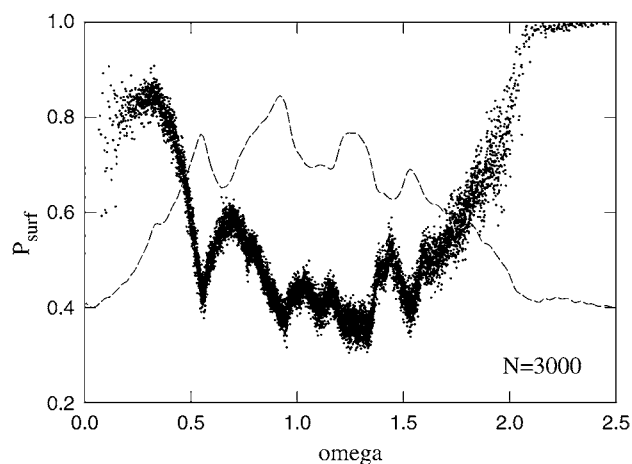
Figure 7. Dots: square modulus P_{surf} of the atomic displacement for the *surface* atoms (see text); dashed line: vibrational density of states for the cluster, rescaled and translated in order to show the correspondence of peaks in P_{surf} and dips in $D(\omega)$.
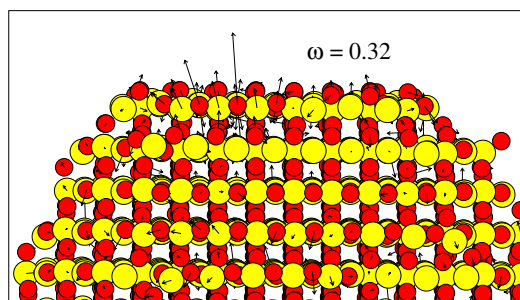

Figure 8. Displacement pattern for a surface localized mode, $N = 3000$.

in $P_{surf}(\alpha)$ appears for each dip in the cluster (or bulk) DOS, documenting the formation of surface modified (either exponentially localized and quasi-localized modes) vibrational states.

A detailed analysis of the eigenvectors shows that surface localized modes in the lowest frequency range appear to be translations and rotations of adatoms or other low coordination atoms at edges and vertices, while the stretching modes of these same atoms account for most of the DOS at the highest frequencies. An example of the displacement pattern for a surface localized mode is shown in figure 8.

Finally, it was verified that a different choice of atomic masses, and in particular one that reproduces more closely the real Ti:O mass ratio, affects the quantitative details in the energy dependence of the DOS and of the vibrational eigenvectors, without changing the qualitative results described above.

4.2. Dielectric properties

The spreading of the IR active modes over a sizable frequency range, which develops as the system size is reduced, is directly related to the size of the oscillating electric dipole moment carried by the modes. This property can be characterized by the frequency distribution, $A(\omega)$,
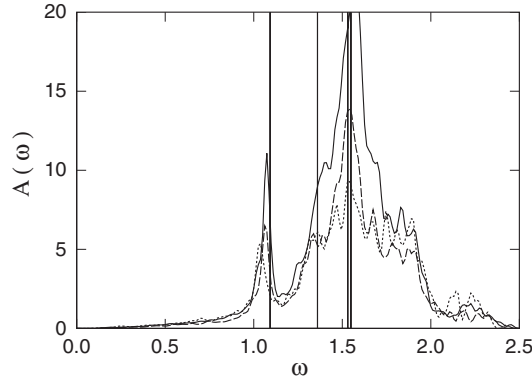
Figure 9. Frequency dependence of the distribution function $A(\omega)$, measuring the (square) dipole strength of vibrational eigenstates (see the definition, equation (6)). Full line: $N = 3000$; dashed line: $N = 1980$; dotted line: $N = 672$. Vertical lines: bulk rutile.

for the square dipole, which is defined as

$$A(\omega) = \sum_{\alpha=1}^{3N} |\mathbf{d}_\alpha|^2 \delta(\omega - \omega_\alpha), \tag{6}$$

where the index α identifies vibrational modes, $\mathbf{d}_\alpha$ is given by

$$\mathbf{d}_\alpha = \sum_{i=1}^{N} Z_i \mathbf{u}_i^{(\alpha)}, \tag{7}$$

and $\mathbf{u}_i^{(\alpha)}$ is the displacement of atom i for the α mode. The completeness of the eigenvector basis implies (*f-sum rule*)

$$\int_0^\infty A(\omega) \, d\omega = 6N. \tag{8}$$

In bulk rutile only the Γ-point phonons contribute to $A(\omega)$, and symmetry constraints imply that only seven modes (corresponding to four non-degenerate frequencies if the LO–TO splitting is neglected) account for the full IR activity strength. The symmetry loss in going from the crystal to the clusters has a drastic effect on $A(\omega)$, as shown in figure 9. The IR active frequencies of the bulk still appear as peaks in the $A(\omega)$ for the clusters, superimposed, however, on a broad background extending from $\omega = 1$ to 2, somewhat blurring the distinction between IR active and inactive modes. Also remarkable is the high frequency tail of $A(\omega)$ for $\omega \geqslant 2.1$, extending well above the highest frequency of IR active, transverse optic modes in bulk rutile. It turns out that these clusters modes are the high frequency modes due to localized surface defects which were discussed in the previous subsection.

The broad distribution of $A(\omega)$ in clusters, strikingly different from its bulk counterpart, has an obvious influence on the frequency dependence of the dipole, $\mathbf{D}(\omega)$, induced by an oscillating perturbing electric field $\mathbf{E}_0 e^{i\omega t}$. Within perturbation theory, the first-order expression for this property is

$$\mathbf{D}(\omega) = \sum_{\alpha=1}^{3N} \mathbf{d}_\alpha \left[\frac{\mathbf{d}_\alpha \cdot \mathbf{E}_0}{m} \right] \frac{1}{\omega_\alpha^2 - \omega^2 + i\eta\omega}, \tag{9}$$

where the sum extends over the vibrational modes and $\mathbf{d}_\alpha$ is defined in equation (7). The parameter η is a (numerically small) dissipation parameter introduced in order to prevent
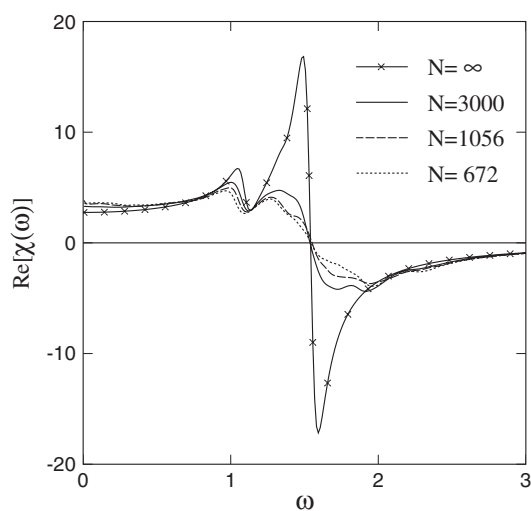
Figure 10. Real part of the complex dipole response function $\chi(\omega)$. Full line: $N = 3000$; dashed line: $N = 1056$; dotted line: $N = 672$; full line with crosses: bulk rutile.

Figure 11. Imaginary part of the complex dipole response function $\chi(\omega)$. Full line: $N = 3000$; dashed line: $N = 1056$; dotted line: $N = 672$; full line with crosses: bulk rutile.
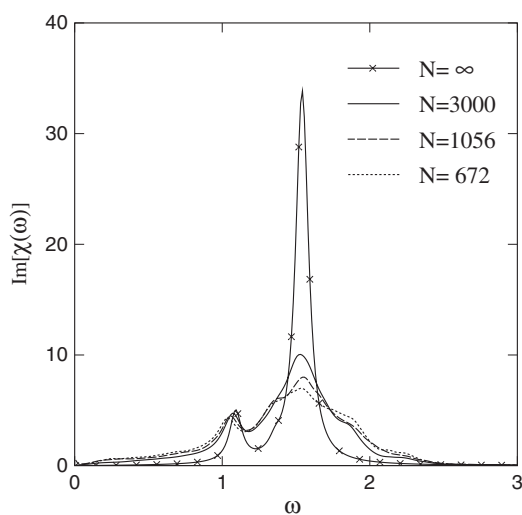
singularities in the dielectric properties. The real part, Re[$\chi(\omega)$], of the corresponding response function $\chi(\omega) = |\mathbf{D}(\omega)|/|\mathbf{E}_0|$ is shown in figure 10 for three different cluster sizes and for bulk rutile. It is evident that this property also converges slowly to the bulk limit, although major features, such as the positions of the peaks, their frequency width, and the zero at $\omega = 1.56$, are already clearly established for $N = 672$. A similar picture is provided by the size dependence of the imaginary part of $\chi(\omega)$, which directly relates to absorption, and is shown in figure 11.
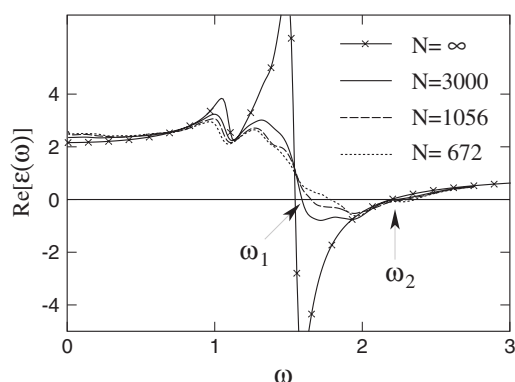
Figure 12. Real part of the effective dielectric constant $\epsilon(\omega)$ (see text). Full line: $N = 3000$; dashed line: $N = 1056$; dotted line: $N = 672$; full line with crosses: bulk rutile. The frequencies ω_1 and ω_2 mark the zeros of $\mathrm{Re}[\epsilon(\omega)]$ for the $N = 3000$ cluster.

The results for $\chi(\omega)$ can be translated in terms of a dielectric function $\epsilon(\omega)$ by using the relation [25]

$$\epsilon(\omega) = 1 + \frac{4\pi}{[V(AB_2)]} \chi(\omega), \tag{10}$$

where $V(AB_2)$ is the volume per molecule of bulk rutile. This definition is obviously only heuristic and approximate, since a dielectric function does not have a rigorous meaning for a finite system, and could be introduced only for cluster-assembled materials. In this last case, however, it would be necessary to include a description of the size-dependent density of the system, and, more importantly, it would be necessary to account for the interactions among the dipoles on different clusters. Nevertheless, even this simple, naïve formulation highlights interesting issues in the dielectric properties of nanometric systems.

The real part $\mathrm{Re}[\epsilon(\omega)]$ of the complex dielectric function $\epsilon(\omega)$ has two zeros at frequencies ω_1 and ω_2 (see figure 12) that identify a frequency range $\omega_1 \leqslant \omega \leqslant \omega_2$ in which the refractive index is imaginary. For a homogeneous system, this would imply that electromagnetic waves cannot propagate within this frequency window. The size of the clusters considered here is too small to give origin to a significant screening of the external field by surface currents. Even for $N = 3000$, a detailed analysis shows that at all frequencies the induced dipole is spread nearly uniformly over the entire cluster.

In homogeneous and cubic crystals having only one longitudinal and two transverse optical modes, the lowest and highest frequency zeros of $\mathrm{Re}[\epsilon(\omega)]$ coincide with the frequency of the transverse and longitudinal optical modes, respectively [25]. It is tempting to interpret the cluster dielectric function in a similar way, attributing to ω_1 and ω_2 the role of an effective (or average) ω_T and ω_L, respectively. Figure 12 clearly shows that, as expected, the size dependence is weak for the longitudinal frequency, determined mainly by short-range repulsive forces, while the size dependence of the transverse frequency is strong, because of its relation with long-range electric fields. The simplest version of the Lyddane–Sachs–Teller relation, which strictly speaking applies only to the simple case mentioned above, states that

$$\epsilon(0) = 1 + \left[\frac{\omega_L}{\omega_T}\right]^2, \tag{11}$$

thus predicting the zero-frequency value of the dielectric function $\epsilon(\omega)$.

Not surprisingly, the computational estimates of ω_T and ω_L for clusters do not satisfy this relation very accurately. Nevertheless, the deviations of the computational results from equation (11) decrease steadily with increasing size, thus providing a direct view of how macroscopic relations arise during the growth of the clusters. For $N = 3000$, for instance, the computational estimates of ω_T ($\equiv \omega_1 = 1.65$) and ω_L ($\equiv \omega_2 = 2.18$) predict a value for $\epsilon(0)$ of 2.75, while the computed value reported in figure 12 is 2.50.

4.3. Stoichiometry effects

Metal oxides represent the technologically most important class of AB_2 materials. These materials, and their surfaces in particular, are well known for their sensitivity to external chemical conditions. Growth of metal oxide clusters in an oxygen deficient ambient easily results in aggregates with oxygen vacancies [9]. A realistic account of this effect strictly requires first principles computations, which include an explicit description of the electronic structure. Nevertheless, here simulations are performed for an idealized model in which N_v of the original $N_- = 2N_+$ negative ions are removed. The cluster is assumed to be neutral, and this is achieved by reducing the charge on N_v positive ions from +2 to +1. The resulting system is therefore made of three species, i.e., $N_+ - N_v$ ions of charge $Z = +2$, N_v ions of charge $Z = +1$, and $2N_+ - N_v$ ions of charge $Z = -1$. In other words, the model assumes that the vacancies are formed via the loss of neutral B atoms (or B_n molecules)[10]. For the sake of simplicity, the short-range interaction of the +2 and +1 ions is assumed to be the same. This assumption and the chosen charge redistribution are arbitrary, and might not approach any real system. This model, however, still represents the simplest prototype of a non-stoichiometric AB_2 system, and it represents an adequate approach for the identification of general consequences of chemical unbalance.

A structural optimization was performed with the method already used for the stoichiometric rutile clusters, this time considering 620 ions of charge $Z = +2$, 40 ions of charge $Z = +1$, and 1280 ions of charge $Z = -1$. The cohesive energy of the $Z = +1$ ions is lower than that of the $Z = +2$ ions, and, as expected, the $Z = +1$ ions segregate at the cluster surface, thus reducing the energy cost due to undercoordination (see figure 13). Repeated structural optimization for the same size never produced a cluster in which a $Z = +1$ ion was not exposed at the surface. Although this result depends on the specific model definitions for the charge distribution and for the short-range interactions, it is apparent that surfaces, edges and vertices are powerful sinks of the defective cations left behind by oxygen vacancies. The steep potential energy barrier for inward diffusion can be compensated by entropy contributions only for large cluster volumes or relatively high temperatures.

Changes in the cluster DOS due to this 3.3% concentration of anion vacancies are quantitatively small but systematic. Because the $Z = +1$ defective cations tend to reside at vertices, and to decorate surface terraces, the sub-stoichiometry mainly affects the frequency of the surface modes identified in section 4.1. More precisely, the replacement of $Z = +2$ with +1 ions decreases the frequency of these modes, and enhances their mixing with extended vibrational states. As a result, peaks and valleys of the DOS are slightly better defined in the defective cluster compared to the stoichiometric case. Moreover, the weight of the highest frequency peak ($\omega > 2.1$) is significantly reduced. The computation of eigenvalues and eigenvectors for the reduced matrix $Q_{\alpha\beta}$ defined in section 4.1 shows that vacancies (at 3.3% concentration) shift the Γ-point vibrational frequencies by $\sim 1.5\%$, irrespective of the IR, Raman or silent character of the corresponding crystal phonon.

---

[10] Referring again to the TiO_2 case, the model assumes that the charge left behind by N_v oxygen vacancies is used to reduce the oxidation state of N_v Ti^{4+} ions, reverting them to Ti^{2+}.
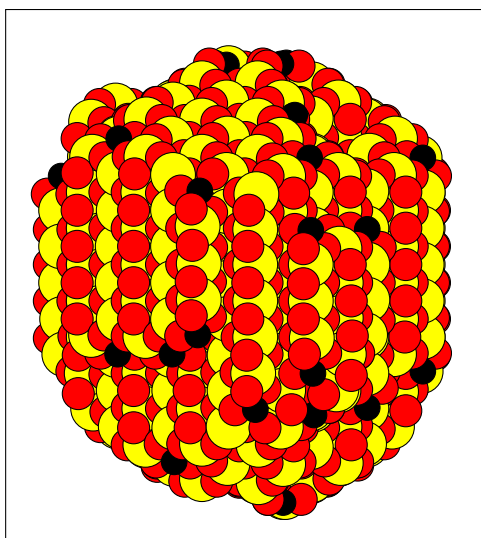
Figure 13. Lowest energy structure of a non-stoichiometric cluster made of 620 cations of charge $Z = +2$ (light grey circles), 40 cations of charge $Z = +1$ (black circles), and 1280 anions (dark grey circles) of charge $Z = -1$. It is intended to model what remains of an $N_A = 660$, $N_B = 1320$ stoichiometric cluster following the loss of 40 neutral B atoms.

The frequency shift of the E_g Raman active mode in TiO$_{2-x}$ nanocrystals have been measured [26] as a function of the oxygen vacancy concentration $100x/2$ (in at.%). A direct comparison with the computational results is not really meaningful, because the model is far too idealized, and its parameters have never been gauged to model TiO$_2$ very closely. Nevertheless, the vacancy-dependent shift of the E_g frequency has the same sign in the experimental and computational results, even though the former is ∼3 times larger than the latter at 3.3% vacancy concentration.

4.4. Cluster-assembled materials: environment effects

The interest in vibrational properties of ionic nanoclusters comes largely from the emerging field of cluster-assembled materials. In these systems, clusters are embedded in a heterogeneous medium made by the other clusters and by voids, in a proportion that depends on the fabrication conditions and on thermodynamic parameters. In most cases, an amorphous matrix is also present, which contributes to the macroscopic cohesion of the system.

For cluster-assembled materials, the medium in which the clusters are embedded could influence their dynamical properties. In order to investigate this effect, here each cluster is thought of as located at the centre of a spherical cavity in an extended dielectric medium of dielectric constant ϵ', which, in general, depends on its average density and stoichiometry. The radius R of the cavity is assumed to be equal to the cluster radius estimated by equation (2). In the case of globally neutral clusters, the dominant potential energy term in a multipole expansion for the cluster–environment interaction is

$$\Delta U = -\frac{\epsilon' - 1}{\epsilon' + 1/2} \frac{\mathbf{d}^2}{R^3},$$ (12)

where $\mathbf{d}$ is the dipole moment of the whole cluster [27].

In the case of gas phase clusters, $\epsilon' = 1$, and this term vanishes identically. In order to represent the general case, the ground state structures discussed in section 4.1 are carefully relaxed and the vibrational frequencies are recomputed upon including ΔU into the Hamiltonian. Computations are performed for $\epsilon' = 5, 30$ and ∞. In all cases, the changes in the equilibrium structures are minor, while the effects on vibrational properties are more important. As expected, changes are more pronounced for the cluster modes related to the IR active Γ-point phonons in the bulk, and their sensitivity to the dielectric properties of the medium is larger for the cluster modes with the strongest IR activity. Furthermore, Raman active and silent modes are also slightly affected since in clusters the strict separation among IR active, Raman active and silent modes is blurred, as mentioned in section 4.1. For $480 \leqslant N \leqslant 3000$ the results show that for $\epsilon' = 30$ the frequency of IR active modes differs by as much as 20% from the case of clusters in the gas phase. Frequency shifts for Raman active and silent modes are typically of the order of 0.5%, and reach up to 1% in the smallest clusters. These frequency shifts are somewhat amplified when the large shift of IR active modes gives rise to level crossings. The frequency shift in the Raman active modes decreases as the clusters size increases because these modes lose their dipole moment as the bulk limit is approached.

These results are strongly reminiscent of the results discussed in early theoretical studies of vibrational properties of finite crystals [5].

5. Concluding remarks

The geometries of AB_2 clusters of size between 480 and 3000 atoms are optimized by using three different methods. Even though the optimization of clusters of this size is a difficult problem, the smooth convergence of cohesive and surface energy as a function of size shows that the geometries found form a representative sample of the growth sequence for this model system.

The vibrational DOS of the smallest cluster already displays the features of the bulk DOS which are dominated by atomic packing constraints and by charge alternation. Convergence of the remaining features as a function of size is slow. A closer comparison with the bulk modes shows that the IR active modes are most affected by the system size, whilst, in general, Raman and silent modes are only weakly affected. A model based on a very simple confinement argument and one based on the surface pressure effect failed to explain the size dependence of the results obtained. In addition, these simple models cannot account for the excess of modes observed at both very low and very high frequencies, which are localized at the surface of the clusters. The low frequency excess modes are found to be localized at edges and vertices, whilst the high frequency modes are due to defects localized on the flat surface regions.

The frequency distribution of the square dipole shows that the sharp separation between IR active and inactive modes that exists in the bulk crystal disappears in the clusters. A heuristic, approximate expression for the dielectric constant is used to illustrate how the distinction between longitudinal and transverse modes, which strictly is defined only for the bulk crystal, slowly emerges as the cluster size increases.

A simple model for sub-stoichiometric clusters is devised by removing part of the negative ions and reducing the charge of some positive ions. Structural optimizations of these modified clusters unfailingly cause the positive ions with reduced charge to segregate at the surface. As a consequence, the sub-stoichiometry of the clusters mainly affects the surface modes, and enhances their mixing with extended vibrational states.

The vibrational properties of the clusters exhibit a dependence on the dielectric constant of the medium in which they are embedded. Once more, the higher the IR activity of the mode, the more sensitive it is to this parameter. Raman active modes show a size-dependent

sensitivity to the dielectric properties of the medium, which gradually disappears as the bulk limit is approached.

Acknowledgments

Appendix

The interpretation of the eigenvalues and eigenvectors of the reduced dynamical matrix $Q_{\alpha\beta}$ (see section 4.1) as representative of the cluster vibrational properties rests on the following observation: by construction, each of the $\beta = 1, \ldots, 18$ eigenvectors corresponds to a unique $3N$-dimensional displacement vector $\mathbf{v}^\beta = \{\mathbf{u}_i^\beta, i = 1, N\}$, in which all the ions in the cluster belonging to the same rutile ion type have the same displacement. Displacing the cluster ions by $\alpha\mathbf{x}$ along an exact vibrational eigenvector $\mathbf{x}$ satisfies the relation

$$\frac{\mathbf{F}(\alpha)}{m} + \omega^2\alpha\mathbf{x} = 0, \tag{13}$$

provided α is small. In the equation above, $\mathbf{F}(\alpha)$ is the $3N$-dimensional force on the ions upon displacing them by $\alpha\mathbf{x}$, and ω is the frequency of the mode whose eigenvector is $\mathbf{x}$. In the case of the $\mathbf{v}^\beta$ displacement vectors the relation (13) is not satisfied, since $\mathbf{v}^\beta$ is not an eigenvector of the full dynamical matrix, but the following inequality is verified for all sizes $N \geqslant 672$ and for all $\beta = 1, \ldots, 18$, provided α is small:

$$\left| \frac{\mathbf{F}(\alpha)}{m} + \omega^2\alpha\mathbf{v}^\beta \right| < 0.08|\alpha\mathbf{v}^\beta|. \tag{14}$$

Moreover, the bound expressed by equation (14) decreases systematically with increasing cluster size. This observation supports the assumption that the eigenvectors of the reduced dynamical matrix provide a meaningful mapping between the cluster vibrational modes and the Γ-point phonons of bulk rutile.

References

[1] Born M and Mayer J E 1932 *Z. Phys.* **75** 1
     Huggins M L and Mayer J E 1933 *J. Chem. Phys.* **1** 643
     Tosi M P 1964 *Solid State Phys.* **16** 1
[2] Ruppin R and Englman R 1970 *Rep. Prog. Phys.* **33** 149 provides a comprehensive review of studies prior to 1970
[3] Frölich H 1949 *Theory of Dielectrics* (Oxford: Clarendon)
[4] Englman R and Ruppin R 1968 *J. Phys. C: Solid State Phys.* **1** 614
[5] Martin T P and Genzel L 1973 *Phys. Rev.* B **8** 1630
[6] See, for instance Martin T P 1978 *J. Chem. Phys.* **69** 2036
     A comprehensive review of early atomistic studies is given in Martin T P 1983 *Phys. Rep.* **95** 167
[7] See, for instance Albaret T, Finocchi F and Noguera C 2000 *Faraday Discuss.* **114** 285
[8] Barborini E, Kholmanov I N, Piseri P, Ducati C, Bottani C E and Milani P 2002 *Appl. Phys. Lett.* **81** 3052
[9] Kholmanov I N, Barborini E, Vinati S, Piseri P, Podestà A, Ducati C, Lenardi C and Milani P 2003 *Nanotechnology* **14** 1168
[10] Zhang H and Banfield J F 1998 *J. Mater. Chem.* **8** 2073
[11] Swamy V and Gale J D 2000 *Phys. Rev.* B **62** 5406 and references therein
[12] Collins D R, Smith W, Harrison N H and Forester T R 1996 *J. Mater. Chem.* **6** 1385

[13] Bulatov V L, Grimes R W and Harker A H 1998 *Phil. Mag. Lett.* **77** 267
[14] Vyas S, Grimes R W, Bulatov V and Abramowski M 2001 *Mol. Simul.* **26** 307
[15] Huang K 1951 *Proc. R. Soc.* A **208** 352
[16] Wille L T and Vennik J 1985 *J. Phys. A: Math. Gen.* **18** L419
[17] Zangwill A 1988 *Physics at Surfaces* (Cambridge: Cambridge University Press)
[18] The first application of genetic algorithms to the optimization of cluster geometries has been reported in
       Deaven D M and Ho K M 1995 *Phys. Rev. Lett.* **75** 288
[19] Diebold U 2003 *Surf. Sci. Rep.* **48** 53
[20] Richter H, Wang Z P and Ley L 1981 *Solid State Commun.* **39** 625
[21] Campbell I H and Fauchet P M 1986 *Solid State Commun.* **58** 739
[22] Dos Santos D R and Torriani I L 1993 *Solid State Commun.* **85** 307
[23] Bersani D and Lottici P P 1992 *Phys. Status Solidi* b **174** 575
[24] The confinement model has been applied to TiO_2 anatase nanocrystals by Bersani D, Lottici P P and
       Ding X-Z 1998 *Appl. Phys. Lett.* **72** 73
[25] Aschroft N W and Mermin N D 1976 *Solid State Physics* (Orlando, FL: Harcourt)
[26] Parker J C and Siegel R W 1990 *Appl. Phys. Lett.* **57** 943
[27] Smith P E and van Gunsteren W F 1993 *Computer Simulation of Biomolecular Systems: Theoretical and
       Experimental applications* vol 2, ed W F van Gunsteren, P K Weiner and A J Wilkinson (Leiden: ESCOM)
       p 182